Experimental characterization of quantum processes: A selective and efficient method in arbitrary finite dimensions

Q. Pears Stefano,[1,2,*] I. Perito,[1,3] J. J. M. Varga,[4,5] L. Rebón,[6] and C. Iemmi[1,2]

[1]*Departamento de Física, FCEyN, Universidad de Buenos Aires, 1428 Buenos Aires, Argentina*
[2]*Consejo Nacional de Investigaciones Científicas y Técnicas (CONICET), 1425 Buenos Aires, Argentina*
[3]*Instituto de Física de Buenos Aires, CONICET, Universidad de Buenos Aires, Facultad de Ciencias Exactas y Naturales, 1428 Buenos Aires, Argentina*
[4]*Centro de Física de Materiales, Paseo Manuel de Lardizabal 5, 20018 Donostia-San Sebastián, Spain*
[5]*Donostia International Physics Center, Paseo Manuel de Lardizabal 4, 20018 Donostia-San Sebastián, Spain*
[6]*Departamento de Física, IFLP–CONICET, Universidad Nacional de La Plata, Casilla de Correo 67, 1900 La Plata, Argentina*

(Received 18 November 2020; revised 15 April 2021; accepted 7 May 2021; published 28 May 2021)

The temporal evolution of a quantum system can be characterized by quantum process tomography, a complex task that consumes a number of physical resources scaling exponentially with the number of subsystems. An alternative approach to the full reconstruction of a quantum channel is the *selective and efficient quantum process tomography*, a method that allows estimating, individually and up to the required accuracy, each element of the matrix that describes the process, using only a polynomial amount of resources. The implementation of this protocol is closely related to the possibility of building a complete set of mutually unbiased bases (MUBs), whose existence is known only when the dimension of the Hilbert space is the power of a prime number. However, an extension of the method that uses tensor products of maximal sets of MUBs has been recently introduced. Here we explicitly describe how to implement the algorithm for a selective and efficient estimation of a quantum process in a nonprime power dimension and conduct, an experimental verification of the method in a Hilbert space of dimension $d = 6$. This is the smallest space for which a complete set of MUBs is not known to exist, but it can be decomposed as a tensor product of two Hilbert spaces of dimensions $D_1 = 2$ and $D_2 = 3$, in which a complete set of MUBs is already known. The six-dimensional states were codified in the discretized transverse linear momentum of photons. The state preparation and detection stages are dynamically programed with the use of only-phase spatial light modulators, in a versatile experimental setup that allows one to implement the algorithm in any finite dimension.

DOI: 10.1103/PhysRevA.103.052438

I. INTRODUCTION

The research in the field of quantum information processing is continuously growing, mainly driven by promising technological applications that range from quantum computation to quantum cryptography and communication [1–5]. On the way to developing reliable quantum technologies, the ability to characterize an unknown quantum device becomes crucial, a task commonly referred to as quantum process tomography (QPT) [6]. This technique is specially useful to experimentally characterize the decoherence mechanisms that take place in noisy quantum gates [7]. For instance, once a given quantum device has been characterized, the *a priori* knowledge of the temporal evolution of any quantum state could be used to design error correction schemes [8].

In this context, different QPT schemes have been tested experimentally for diverse physical implementations of quantum systems: polarization of photons [9–11], superconducting qubits [12,13], nuclear-magnetic-resonance quantum computers [14], and ion traps [15], among others. However, since this is considered a *hard task* due to the required physical resources, the research for efficient schemes becomes more and more relevant as the size of experimentally feasible systems increases.

Within the formalism of quantum mechanics the state of a physical system is described by a density matrix, ρ, and the quantum operation of a device can be mathematically represented by a linear, completely positive map, $\mathcal{E}$, that applied over a quantum state ρ_{in} returns the state $\rho_{\text{out}} = \mathcal{E}(\rho_{\text{in}})$ [16]. The effect of this map can always be written in the so-called *operator-sum representation* or *Kraus decomposition* as

$$\mathcal{E}(\rho) = \sum_i A_i \rho A_i^\dagger, \tag{1}$$

where $\{A_i\}_i$ is a set of linear operators that act on a Hilbert space, $\mathcal{H}$, and satisfy the relation $\sum_i A_i A_i^\dagger \leqslant \mathbb{I}$. If the dimension of the system under consideration is d, one can choose a basis of operators, $\{E_m, m = 0, \ldots, d^2 - 1\}$, and rewrite Eq. (1) as

$$\mathcal{E}(\rho) = \sum_{mn} \chi_{mn} E_m \rho E_n^\dagger, \tag{2}$$

where χ is a Hermitian and positive matrix and the trace-preserving condition is given by $\sum_{mn} \chi_{mn} E_n^\dagger E_m = \mathbb{I}$. Once the operator basis $\{E_m\}$ is fixed, performing QPT is equivalent to

*quimeyps@df.uba.ar

 ©2021 American Physical Society

determining the matrix coefficients χ_{mn}'s. Therefore, the full characterization of the map requires $d^4 - d^2$ real parameters, and in the case of n-qubit systems, this is associated with an exponentially large number of coefficients to be determined ($d = 2^n$). Moreover, standard methods require an amount of experimental and computational resources that scale exponentially with the number n of subsystems, even to determine a single coefficient. In this context, a protocol for quantum process tomography is said to be

(i) *selective*, if it allows one to obtain, individually, the coefficients of the matrix χ, i.e., without having to perform the full QPT in case we are only interested in some particular element χ_{mn}, and

(ii) *efficient*, if any coefficient χ_{mn} can be determined with subexponential resources.

In previous works [17,18], a protocol for selective and efficient quantum process tomography (SEQPT) was developed and successfully accomplished experimentally on different physical platforms [19,20]. However, the protocol is implementable as long as the dimension of the Hilbert space is the power of a prime number. This is because the SEQPT makes use of a complete set of mutually unbiased bases (MUBs), a construction which is only known to exist for prime-power dimensions [21–23].

More recently, two schemes that allow extending the SEQPT protocol to arbitrary finite dimensions were presented in Ref. [24]. One of these scheme is based on tensor products of complete sets of MUBs in lower prime-power dimensions, as a good approximation to solve the original problem. The other one starts from a complete set of MUBs in a higher dimension and then projects this set onto the desired dimension. Which strategy to follow will depend mainly on the physical implementation: the SEQPT with tensor product, for example, requires the preparation of product states in smaller dimensions and it could be the most suitable option for composite systems, although there is no advantage over the SEQPT with projection in relation to the number of individual experiments required to estimate a given coefficient.

In this work, we present the experimental realization of the tensor product scheme for the SEQPT protocol. The method is applied to characterize a trace-preserving quantum process on dimension $d = 6$, that is, the smallest Hilbert space for which the protocol for SEQPT in a nonpower prime dimension becomes relevant. Among the many possible codifications for a quantum state of dimension d (qudit), the spatial degrees of freedom of a single photon provide an easy access to dimensions $d \geqslant 2$. In particular, here we have encoded the d-dimensional system in the discretized transverse momentum of single photons, a scheme widely used for implementing quantum information processing in high dimensions [25–27] and which has proven useful for testing protocols for both quantum state tomography [28,29] and quantum process tomography [30].

The paper is organized as follows. In Sec. II we briefly describe the main idea behind the SEQPT protocols, with particular emphasis in the tensor product scheme for the case of dimensions with two different prime numbers in their factorization, given that this is the case on which we focus throughout our experiment. After that, in Sec. III, we describe the experimental setup and, finally, in Sec. IV we present our results and conclusions.

II. SEQPT METHOD

Let us first briefly review the theoretical background for the SEQPT protocol in prime power dimensions [17,18] and its generalization to a more general case when the dimension is factorized as a product of two prime power dimensions [24].

A. Haar integrals of quadratic forms and 2-designs

The protocol for SEQPT that we implement in this work is based on the following properties.

(i) For any two operators, A and B, in a Hilbert space, $\mathcal{H}$, of dimension d, it holds that

$$\int_{\mathcal{H}} d\psi \, \mathrm{Tr}[P_\psi \, A \, P_\psi B] = \frac{\mathrm{Tr}A \, \mathrm{Tr}B + \mathrm{Tr}[AB]}{d(d+1)}, \tag{3}$$

where $P_\psi = |\psi\rangle\langle\psi|$, and the integration is performed over the only measure that is unitarily invariant and normalized on $\mathcal{H}$, namely, the Haar measure.

(ii) A finite set of states $\mathcal{X} = \{|\psi_m\rangle, m = 1, \ldots, N\}$ is a uniform state 2-design if

$$\int_{\mathcal{H}} d\psi \, f(P_\psi) = \frac{1}{N} \sum_{m=1}^{N} f(P_{\psi_m}) \tag{4}$$

for any f that is quadratic in P_ψ and the integration is performed again over the Haar measure.

Therefore, a state 2-design is a set of states on which the mean value of any quadratic function in P_ψ gives the same mean value as on the set of all possible states in $\mathcal{H}$. Note that, in particular, this kind of set allows one to easily compute quantities in Eq. (3).

B. Quantum channel fidelity and SEQPT in prime power dimension

Given the quantum channel $\mathcal{E}$, its mean fidelity is given by

$$\bar{F}(\mathcal{E}) = \int_{\mathcal{H}} d\psi \, \mathrm{Tr}[P_\psi \, \mathcal{E}(P_\psi)], \tag{5}$$

where the integration is taken over the Haar measure. According to Eq. (2) we expand $\mathcal{E}$ by selecting an operator basis $\{E_m\}$ that is orthogonal [$\mathrm{Tr}(E_m E_n^\dagger) = d\delta_{m,n}$] and unitary ($E_n E_n^\dagger = \mathbb{I}$). If we define the modified channel as

$$\mathcal{E}_{ij}(\rho) \equiv \mathcal{E}(E_i^\dagger \rho E_j), \tag{6}$$

a direct application of the property given by Eq. (3) relates the mean fidelity of $\mathcal{E}_{ij}$ with the element χ_{ij} of the matrix description of the channel $\mathcal{E}$. We focus here on trace-preserving maps, i.e., where the condition $\sum_i A_i A_i^\dagger = \mathbb{I}$ is held. In such a particular case, the relation is explicitly

$$\bar{F}(\mathcal{E}_{ij}) = \frac{d \, \chi_{ij} + \delta_{ij}}{d+1}. \tag{7}$$

Moreover, given that the mean fidelity is the integral over the Haar measure of a quadratic form in P_ψ, it can be computed just by evaluating and averaging the survival probability, through the channel $\mathcal{E}_{ij}$, over the states of a 2-design,

$\bar{F}(\mathcal{E}_{ij}) = \frac{1}{N}\sum_{m=1}^{N} \mathrm{Tr}[|\psi_m\rangle\langle\psi_m|\,\mathcal{E}(E_i^\dagger|\psi_m\rangle\langle\psi_m|E_j)]$. This finally gives the clue along with Eq. (7) to design the experiments to find the desired coefficients χ_{ij}, once a a 2-design is known.

A simple way to find a state 2-design is to consider a set of $(d+1)$ MUBs, which automatically form a state 2-design [31] and their construction is known when the dimension d is the power of a prime number [21,22]. However, for arbitrary dimension d, the maximum number of MUBs is not known.

C. SEQPT in arbitrary finite dimension

In the general case, the previous protocol fails because of the lack of a uniform 2-design when the dimension of the system d is not the power of a prime number. However, two strategies that allow the generalization of the SEQPT protocol to an arbitrary dimension were recently presented in Ref. [24]. They consist of finding a finite set of states that, despite not being a uniform 2-design, allows one to compute mean fidelities in a reasonable way. In particular, we follow the tensor product approach based on the fact that tensor products of 2-designs can be used to approximate 2-designs. Since an arbitrary dimension d can always be factorized into the power of prime numbers, then the tensor products of maximal MUB sets provide a good approximation for integration purposes.

We focus on the bipartite case in which we are concerned in this work. In such a case, the dimension of the Hilbert space d is factorized as $d = D_1 D_2$, where $D_1 = p_1^{n_1}$, $D_2 = p_2^{n_2}$, and p_1 and p_2 are prime numbers. The first step is to expand the channel $\mathcal{E}$ in a basis that is a product of operators acting on $\mathcal{H} = \mathcal{H}_1 \otimes \mathcal{H}_2$, where the dimensions of the subsystems are D_1 and D_2, respectively. This basis can be written in terms of two orthogonal operator bases $\{E_{j_1 j_2} \equiv E_{j_1} \otimes E_{j_2}\}_{j_1=0,\ldots,D_1^2-1}^{j_2=0,\ldots,D_2^2-1}$, where each element E_{j_i} ($i = 1$ and 2) is a unitary matrix. Thus, the expansion in Eq. (2) is rewritten as

$$\mathcal{E}(\rho) = \sum_{\mu_1\mu_2\nu_1\nu_2} \chi_{\nu_1\nu_2}^{\mu_1\mu_2} E_{\mu_1\mu_2}\rho E^{\nu_1\nu_2}, \tag{8}$$

for some coefficients $\chi_{\nu_1\nu_2}^{\mu_1\mu_2}$. We have adopted the conventions $E^{j_i} \equiv E_{j_i}^\dagger$ and $E^{j_1 j_2} \equiv E_{j_1 j_2}^\dagger$, and hereafter, we also consider $\delta_i^j \equiv \delta_{ij}$. If we take X_1 and X_2 as 2-designs in $\mathcal{H}_1$ and $\mathcal{H}_2$, respectively, and define $X_\otimes \subset \mathcal{H}_1 \otimes \mathcal{H}_2$ as the set of all possible tensor product between states in X_1 and states in X_2, the coefficient $\chi_{j_1 j_2}^{i_1 i_2}$ can be expressed as

$$\chi_{j_1 j_2}^{i_1 i_2} = \bar{F}_\otimes\big(\mathcal{E}_{j_1 j_2}^{i_1 i_2}\big)\frac{(1+D_1)(1+D_2)}{d} + \frac{\delta_{j_1}^{i_1}\delta_{j_2}^{i_2}}{d} - \bar{F}_1\big(\mathcal{E}_{j_1 j_2}^{i_1 i_2}\big)\frac{(1+D_1)}{d} - \bar{F}_2\big(\mathcal{E}_{j_1 j_2}^{i_1 i_2}\big)\frac{(1+D_2)}{d}, \tag{9}$$

where the modified channel is now given by $\mathcal{E}_{j_1 j_2}^{i_1 i_2}(\rho) = \mathcal{E}(E^{i_1 i_2}\rho E_{j_1 j_2})$. The mean fidelity of this modified channel is expressed as

$$\bar{F}_\otimes\big(\mathcal{E}_{j_1 j_2}^{i_1 i_2}\big) = \int_{\mathcal{H}_1}\int_{\mathcal{H}_2} d\psi_1 d\psi_2\, \mathrm{Tr}\big[P_{\psi_1\psi_2}\,\mathcal{E}_{j_1 j_2}^{i_1 i_2}(P_{\psi_1\psi_2})\big], \tag{10}$$

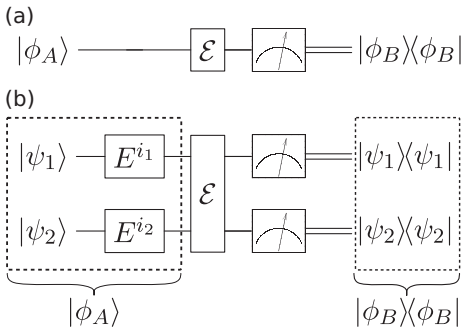

FIG. 1. (a) Circuit for a projective measurement of state $|\phi^A\rangle$, after being affected by the process $\mathcal{E}$, onto the state $|\phi^B\rangle$. (b) Circuit for measuring the survival probability of the state $|\psi\rangle = |\psi_1\rangle \otimes |\psi_2\rangle$ through the modified channel $\mathcal{E}_{i_1 i_2}^{i_1 i_2}$. By sampling over $X_\otimes$ we can obtain the diagonal element $\chi_{j_1 j_2}^{i_1 i_2}$ corresponding to the process matrix of $\mathcal{E}$.

and this double integral can be evaluated by averaging over the finite set of states in $X_\otimes$:

$$\bar{F}_\otimes\big(\mathcal{E}_{j_1 j_2}^{i_1 i_2}\big) = \frac{1}{|X_1|}\frac{1}{|X_2|}\sum_{|\psi_1\rangle\in X_1}\sum_{|\psi_2\rangle\in X_2}\mathrm{Tr}\big[P_{\psi_1\psi_2}\,\mathcal{E}_{j_1 j_2}^{i_1 i_2}(P_{\psi_1\psi_2})\big] = \frac{1}{|X_\otimes|}\sum_{|\psi\rangle\in X}\mathrm{Tr}\big[P_\psi\,\mathcal{E}_{j_1 j_2}^{i_1 i_2}(P_\psi)\big]. \tag{11}$$

Furthermore, measuring the action of the modified channel over the states in $X_\otimes$ is enough to compute, not only $\bar{F}_\otimes(\mathcal{E}_{j_1 j_2}^{i_1 i_2})$, but *all* the terms in Eq. (9). For instance, in order to estimate the reduced mean fidelity over subsystem X_1,

$$\bar{F}_1\big(\mathcal{E}_{j_1 j_2}^{i_1 i_2}\big) = \int_{\mathcal{H}_1} d\psi_1 \langle\psi_1|\mathrm{Tr}_2\big[\mathcal{E}_{j_1 j_2}^{i_1 i_2}(P_{\psi_1}\otimes\mathbb{I}_2/D_2)\big]|\psi_1\rangle, \tag{12}$$

one has to measure the survival expectation of $P_{\psi_1}\otimes\mathbb{I}_2$ given the initial state $P_{\psi_1}\otimes\frac{\mathbb{I}_2}{D_2}$, that is,

$$\bar{F}_1\big(\mathcal{E}_{j_1 j_2}^{i_1 i_2}\big) = \frac{1}{|X_1|}\sum_{|\psi_1\rangle\in X_1}\mathrm{Tr}\big[(P_{\psi_1}\otimes\mathbb{I}_2)\mathcal{E}_{j_1 j_2}^{i_1 i_2}(P_{\psi_1}\otimes\mathbb{I}_2/D_2)\big]. \tag{13}$$

It can be achieved by looking at the statistics of the measurements on system 1 independently from the results of the measurements on system 2, and similarly for $\bar{F}_2(\mathcal{E}_{j_1 j_2}^{i_1 i_2})$. This is because the initial state of system 2 is a random state from $(1+D_2)$ orthogonal bases, which is a possible implementation of $\mathbb{I}_2$ provided the result of the measurement of system 2 is not taken into account. Thus, the selectivity of the method is given by the fact that a particular element $\chi_{i_1 i_2}^{j_1 j_2}$ can be determined by calculating the three mean fidelities $\bar{F}_\otimes$, $\bar{F}_1$, and $\bar{F}_2$, over the modified channel $\mathcal{E}_{i_1 i_2}^{j_1 j_2}$. Furthermore, these fidelities can be estimated *efficiently* by randomly sampling states in $X_\otimes$: given a fixed error tolerance, the number of states to be sampled is independent of the dimension.

Figure 1 depicts the procedure to follow in the reconstruction of a given coefficient $\chi_{j_1 j_2}^{i_1 i_2}$. Let us assume that we have an experimental setup described by the circuit in Fig. 1(a) where an arbitrary state $|\phi^A\rangle$ is prepared and, after being affected by the process $\mathcal{E}$, it is projected onto the state $|\phi^B\rangle$.

Diagonal case. For $i_1 = j_1$ and $i_2 = j_2$, the effect of the modified channel on the state $|\psi\rangle = |\psi_1\rangle \otimes |\psi_2\rangle \in X_\otimes$ is

$$\begin{aligned}\mathcal{E}^{i_1 i_2}_{i_1 i_2}(|\psi\rangle\langle\psi|) &= \mathcal{E}\big(E^{i_1 i_2}|\psi\rangle\langle\psi|E_{i_1 i_2}\big) \\ &= \mathcal{E}\big(E^{i_1}P_{\psi_1}E_{i_1} \otimes E^{i_2}P_{\psi_2}E_{i_2}\big),\end{aligned} \tag{14}$$

and the survival expectation can be obtained by performing a projective measurement onto $|\psi_1\rangle \otimes |\psi_2\rangle$. The circuit describing this procedure is shown in Fig. 1(b), where now the input state is $|\phi^A\rangle = E^{i_1 i_2}|\psi\rangle$ and the state to be projected onto is $|\phi^B\rangle = |\psi\rangle$. An explicit construction of the 2-designs X_1 and X_2 and the corresponding operator bases is discussed in Sec. III.

Nondiagonal case. For $i_1 \neq j_1$ or $i_2 \neq j_2$, the resulting modified channel is nonphysical. In fact, its effect on the sampled state $|\psi\rangle$ is given by

$$\begin{aligned}\mathcal{E}^{i_1 i_2}_{j_1 j_2}(|\psi\rangle\langle\psi|) &= \mathcal{E}(E^{i_1 i_2}|\psi\rangle\langle\psi|E_{j_1 j_2}) \\ &= \mathcal{E}(|\alpha\rangle\langle\beta|),\end{aligned} \tag{15}$$

with $|\alpha\rangle = E^{i_1 i_2}|\psi\rangle$ and $|\beta\rangle = E_{j_1 j_2}|\psi\rangle$. This is equivalent to the action of the original channel $\mathcal{E}$ on the matrix $|\alpha\rangle\langle\beta|$, which is not a density matrix, and therefore does not represent a physical state. However, this matrix can always be expressed as a linear combination of *at most* five matrices, each corresponding to a projector. If $|\alpha\rangle$ and $|\beta\rangle$ are orthonormal, $\mathcal{E}(|\alpha\rangle\langle\beta|) = \mathcal{E}(|+\rangle\langle+|) + \mathcal{E}(|-\rangle\langle-|) - \frac{1+i}{2}[\mathcal{E}(|\alpha\rangle\langle\alpha|) + \mathcal{E}(|\beta\rangle\langle\beta|)]$, with $|+\rangle = (|\alpha\rangle + |\beta\rangle)/\sqrt{2}$ and $|-\rangle = (|\alpha\rangle + i|\beta\rangle)/\sqrt{2}$. If they are not orthonormal, a similar decomposition exists. Then, the linearity of $\mathcal{E}$ ensures that we can compute the action of the modified channel $\mathcal{E}^{i_1 i_2}_{j_1 j_2}$ over any state as a linear combination of the action of the original channel $\mathcal{E}$ over a suitable choice of pure states.

III. EXPERIMENTAL TENSOR PRODUCT SEQPT

In order to experimentally test the tensor product SEQPT protocol, we have implemented and reconstructed a quantum process $\mathcal{E}$ in a Hilbert space of dimension $d = 6$, for which a maximal set of MUBs is not known. In our case, $\mathcal{E}$ is a nontrivial process over qudit states encoded in the discretized transverse position of single photons [32].

For this encoding, a d-dimensional quantum state can be defined by means of a complex aperture consisting of d slits and placed in the path propagation of the photon field, so that the dimension of the spatial qudit is determined by the number of paths available to the photon. To be more specific, when such an aperture is illuminated by a paraxial and monochromatic single-photon field, which is approximately constant on the aperture area, the resulting state—usually called the *slit state*—can be described by

$$|\psi\rangle = \frac{1}{\mathcal{N}}\sum_{k=0}^{d-1} c_k|k\rangle, \tag{16}$$

where c_k is the complex transmission of the kth slit, $|k\rangle$ represents the transverse-path state of a single photon through this slit, and the normalization constant is given by $\mathcal{N} = \sqrt{\sum_{i=0}^{d-1}|c_i|^2}$. Optically, $|c_k|^2$ and $\arg(c_k)$ correspond to the intensity transmission and the phase retardation of the k slit, respectively, which can be independently controlled by defining the complex aperture in a programmable spatial light modulator (SLM) [33,34].

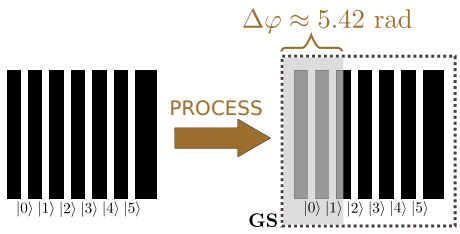

FIG. 2. Effect of the process on the six-dimensional spatial qudit codified in the discretized transverse momentum of a photon. The process is physically implemented by a glass slab (GS) with a transparent coating covering part of its surface. This partial coating introduces a phase shift $\Delta\varphi = 5.42$ rad on the paths that codify the states $|0\rangle$ and $|1\rangle$ of the six-dimensional canonical basis.

We made the following assignments between states in the canonical basis of $d = 6$ and tensor products of the elements in the canonical bases of $D_1 = 2$ and $D_2 = 3$:

$$\begin{aligned}|0\rangle &\to |0\rangle \otimes |0\rangle\ , \quad |3\rangle \to |1\rangle \otimes |0\rangle, \\ |1\rangle &\to |0\rangle \otimes |1\rangle\ , \quad |4\rangle \to |1\rangle \otimes |1\rangle, \\ |2\rangle &\to |0\rangle \otimes |2\rangle\ , \quad |5\rangle \to |1\rangle \otimes |2\rangle.\end{aligned} \tag{17}$$

According to this, the state in Eq. (16) is rewritten as

$$|\psi\rangle = \frac{1}{\mathcal{N}}\sum_{k_1=0}^{D_1-1}\sum_{k_2=0}^{D_2-1} c_{k_1 k_2}|k_1\rangle \otimes |k_2\rangle. \tag{18}$$

The target process to be implemented corresponds to add a constant phase shift, $\Delta\varphi$, to the states $|0\rangle$ and $|1\rangle$ of the canonical basis in $d = 6$. For this process, a decomposition in terms of Kraus operators is

$$\begin{aligned}\mathcal{E}_t(\rho) &= A_t \rho A_t^\dagger, \\ A_t &= e^{i\Delta\varphi}(|0\rangle\langle 0| + |1\rangle\langle 1|) + \sum_{k=2}^{5}|k\rangle\langle k|.\end{aligned} \tag{19}$$

Physically, this was realized by means of a rectangular glass slab (GS) partially coated with a transparent material, resulting in an extra phase of $\Delta\varphi = 5.42$ rad for the wavelength that was used in our experiment. Figure 2 shows, schematically, the effect of the target process $\mathcal{E}_t$ when acting on a state generated by a six-slit aperture.

The experimental setup is shown in Fig. 3. It is a flexible configuration that allows us to generate arbitrary pure states and perform general projective measurements based on the use of phase-only SLMs [34]. It can be divided in two main parts: the state preparation part (SP), in which the state $|\phi^A\rangle$, which subsequently crosses the channel, is prepared, and the process tomography part (PT), where we select the state $|\phi^B\rangle$ onto which $\mathcal{E}_t(|\phi^A\rangle\langle\phi^A|)$ will be finally projected.

Let us describe the SP part. The light source is a laser diode @405 nm that is expanded and collimated by the microscope objective O and the lens L_c, respectively. Neutral density filters, not shown in the figure, were used to test the proposed technique at the single-photon level. Each state was prepared with a total optical power lower than 0.02 nW

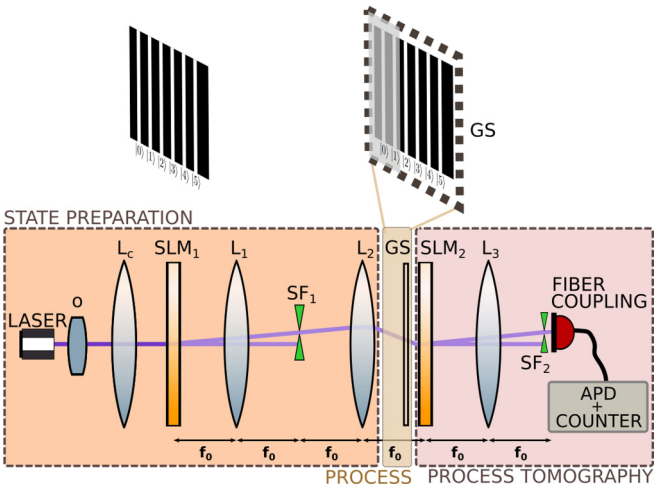

FIG. 3. Experimental setup. A 405-nm cw laser diode is attenuated to the single-photon level. O, microscope objective; Ls, convergent lenses; SLMs, pure-phase spatial light modulators; SFs, spatial filters. A glass slab (GS) implements the process on a spatial qudit as schematized in Fig. 2. The detection in the center of the interference pattern is performed with a fiber-coupled avalanche photodiode (APD).

(measured after SF1). Taking into account the time it takes for a photon to travel the experimental length to the detector (∼100 cm), we can assume that, on average, there is less than one photon present throughout the experiment. Although this is not a proper single-photon source, it is enough to test the feasibility of quantum state estimation methods [35–37]. The complex aperture that generates each qudit $|\phi^A\rangle$ is displayed in the phase-only SLM_1, which is uniformly illuminated by the collimated incoming beam. This SLM consists of a twisted nematic liquid crystal display (LCD) Sony LCX012B coupled to polarizers and wave plates. By selecting suitable polarization states [38], both at the input and the output of the LCD, a phase-only modulation of 2π @405 nm on the wave front is attained. This LCD has a VGA resolution (640×480) with pixels of 43 μm per side. The displayed slits were defined to have a width of 172 μm (4 pixels) and a separation of 258 μm (6 pixels) between their centers.

To control independently the complex amplitude of every slit—transmissivity and phase retardation—with a phase-only SLM, we implement the method described in Ref. [34]. Briefly, this is achieved by programming a different-phase grating in the spatial region corresponding to each slit, orientated along its main length. The phase-depth of the grating (Φ_0) determines the efficiency, η_1, of the first diffraction order, following the equation

$$\eta_1 = \mathrm{sinc}^2\left(\frac{1}{p}\right)\frac{\mathrm{sinc}^2\left(1-\frac{\Phi_0}{2\pi}\right)}{\mathrm{sinc}^2\left(\frac{1-\frac{\Phi_0}{2\pi}}{p}\right)}, \tag{20}$$

where p is the grating period in pixels. In our case the period was selected to be 344 μm ($p = 8$ pixels). Hence, the real amplitude of c_k in the superposition of Eq. (16) is codified by the efficiency of the kth grating, while the complex argument, $\arg(c_k)$, corresponds to the constant additive phase for that slit. Finally, a spatial filter is needed to select the first diffracted order, in which the state was codified. For this purpose, the lenses L_1 and L_2 (both of focal length $f_0 = 26$ cm), together with the spatial filter SF_1, constitute the $4-f$ optical processor that selects this diffracted order. Thus, at the back focal plane of L_2, the wave-front distribution corresponds to the desired spatial qudit.

In the PT part, a second SLM (SLM_2), with characteristics similar to those of SLM_1 and operating in the same way, encodes each projection base state $|\phi^B\rangle$. In the absence of the channel $\mathcal{E}_t$ implemented by means of a GS, if $|\phi^B\rangle = \sum b_k|k\rangle$ the resulting state after SLM_2 is proportional to $\sum c_k b_k^*|k\rangle$ (considering that $|\phi^A\rangle = \sum c_k|k\rangle$). This second SLM is placed at the front focal plane of lens L_3. After filtering the first diffracted order by means of SF_2, the exact Fourier transform of the projected spatial qudit is obtained at the detector plane. The light distribution corresponds to the interference pattern projection between the prepared state and the selected projector state. The light from the center of this pattern is coupled by a single-mode fiber into a single-photon counting module, Perkin Elmer SPCM-AQRH-13-FC, based on an avalanche photodiode (APD). Then, the single-photon count rate is proportional to the probability of projection of the two states, $p(|\phi^A\rangle, |\phi^B\rangle)$ [36]. In the presence of the channel $\mathcal{E}_t$, this probability will be $p[\mathcal{E}(|\phi^A\rangle\langle\phi^A|), |\phi^B\rangle]$.

Bases of the operator space and MUBs

To expand the channel $\mathcal{E}$ we have chosen two bases of unitary operators acting on $\mathcal{H}_1$ and $\mathcal{H}_2$, respectively. The selected bases are the well-known Sylvester's bases [39,40], which for any dimension d can be written as

$$E_n \equiv E_{kl} = \sum_{m=0}^{d-1} \omega^{ml}|m \oplus k\rangle\langle m|, \tag{21}$$

where $k, l = 0, \ldots, d-1$, $\omega = \exp(2\pi i/d)$ is a root of unity, and $\oplus$ is the modulo-d addition.

For the case $d = D_1 = 2$, the four operators are simply

$$E_{00} = \mathbb{I}, \quad E_{01} = \sigma_z, \quad E_{10} = \sigma_x, \quad E_{11} = i\sigma_y, \tag{22}$$

from which we can obtain three abelian sets of two elements each: $\{E_{00}, E_{01}\}$, $\{E_{00}, E_{10}\}$, and $\{E_{00}, E_{11}\}$. The three bases that diagonalize each of these sets, i.e., the three bases of eigenvectors of the Pauli operators, not only give a complete set of MUBs for $d = 2$ (and, hence, a proper 2-design) but also have the property that the action of any of the four operators E_{kl} over any of the elements in the 2-design gives another element within the same MUB basis, except for a global phase. In fact, if $|\psi_m^j\rangle$ is one of the d elements within the j MUB, the following property is verified:

$$E_{kl}\left|\psi_m^j\right\rangle = e^{i\alpha(k,l,m,j)}\left|\psi_{m'}^j\right\rangle. \tag{23}$$

In the case that $d = D_2 = 3$, we can analogously obtain a 2-design by extracting four abelian subsets from the nine operators E_{kl}. The first of them, $\{E_{00}, E_{01}, E_{02}\}$, is diagonalized by the canonical basis

$$\mathcal{B}_1 = \{|0\rangle, |1\rangle, |2\rangle\} \equiv \{(1,0,0), (0,1,0), (0,0,1)\}. \tag{24}$$

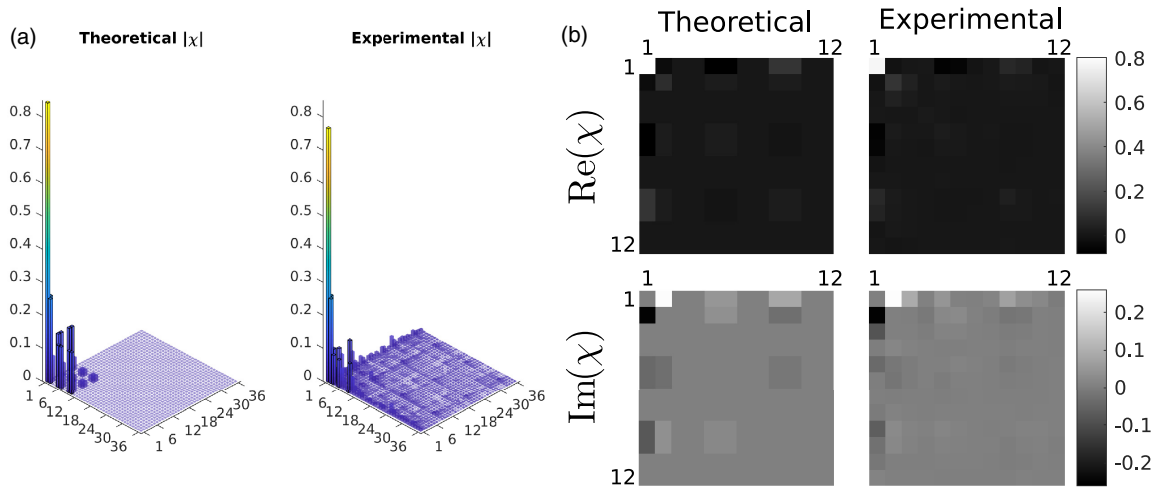

FIG. 4. (a) Comparison of the absolutes values of the elements of χ_{theo} (expected matrix of the target process $\mathcal{E}_t$) and χ_{exp} (reconstructed by the tensor product SEQPT). (b) Detail of the absolute value of the elements in the 12×12 submatrix. This elements correspond to the nonzero block in the matrix χ_{theo} [upper-left block in the theoretical plot of panel (a)]. The gray-scale map shows the real and imaginary part for the theoretical and the experimental reconstructed matrices.

The next set, $\{E_{00}, E_{10}, E_{20}\}$, is diagonalized by

$$\mathcal{B}_2 = \left\{ \frac{(1,1,1)}{\sqrt{3}}, \frac{(1,\omega,\omega^2)}{\sqrt{3}}, \frac{(1,\omega^2,\omega)}{\sqrt{3}} \right\}, \tag{25}$$

where $\omega = \exp(2i\pi/3)$, $\omega^2 = \omega^*$, and $\omega^3 = 1$. It is clear that $\mathcal{B}_1$ and $\mathcal{B}_2$ are mutually unbiased. Moreover, by taking $\mathcal{B}_3$ and $\mathcal{B}_4$ as the bases that diagonalize the sets $\{E_{00}, E_{11}, E_{22}\}$ and $\{E_{00}, E_{12}, E_{21}\}$, respectively, we get four MUBs in $d = 3$ and hence a 2-design in the corresponding Hilbert space. Again, it is easy to check that the property given by Eq. (23) holds for the nine operators E_{kl}.

As in the case of the present work, if the 2-designs in each subsystem X_1 and X_2 are chosen as the complete sets of MUBs obtained above, the action of any element of the operator basis over any element of $X_\otimes$ gives, by construction, another element of $X_\otimes$. Thus, the experimental implementation of the *modified* quantum channel $\mathcal{E}_{j_1 j_2}^{i_1 i_2}$ only requires preparing products of the 2-design elements as input states $|\phi_A\rangle$ (Fig. 1).

IV. RESULTS AND DISCUSSION

To evaluate the viability of the method, we first performed the full tomography of the process $\mathcal{E}_t$ introduced in our experimental setup by means of a GS. To this end we have reconstructed each coefficient of the matrix, $\chi_{j_1 j_2}^{i_1 i_2}$, by averaging over all the elements of the tensor product of the 2-design $X_\otimes$ [see Eqs. (9)–(13)]. Given the particular product of the 2-design and the basis for the operator space that we have selected (see Sec. III), some of the measurement settings are repeated. This results in a total of 2592 projections to perform the full reconstruction. Each projection was measured for a period of time $\Delta t = 166$ ms, with a maximum number of registered photocounts of approximately 20×10^3 per projection, which results in a total tomographic time of about 1 hr.

The experimental matrix χ_{exp} was postprocessed with the complete positive trace-preserving projection (CPTP) algorithm presented in Ref. [41]. This projection ensures that the resulting matrix is completely positive. Then, it represents a physical process and the trace of any quantum state is preserved. The last constraint is in agreement with the target process $\mathcal{E}_t$. Figure 4(a) shows the comparison between the absolute values of the elements of the theoretical matrix χ_{theo} and χ_{exp} in the measurement basis. For a better comparison, Fig. 4(b) shows a detail of the nonzero 12×12 block of the expected matrix comparing both the real [$\text{Re}(\chi)$] and the imaginary [$\text{Im}(\chi)$] parts of χ_{theo} and χ_{exp}. As a figure of merit and resorting to the Choi-Jamiolkowski isomorphism [6], we calculate the similitude between χ_{theo} and χ_{exp} as the fidelity $F \equiv F(\rho_{\text{theo}}, \rho_{\text{exp}}) = \text{Tr}\sqrt{\sqrt{\rho_{\text{theo}}}\rho_{\text{exp}}\sqrt{\rho_{\text{theo}}}}$ between two quantum states, ρ_{theo} and ρ_{exp}, assigned to the target process and to the experimentally reconstructed one ($\mathcal{E}_{\text{exp}}$), respectively. The obtained value, which is essentially a measure of the geometrical proximity in the Hilbert space, is $F = 0.932$. For completeness and to make the reconstruction quality of the method independent of the errors inherent to the experimental setup, we have also performed the standard established method for quantum process tomography (standard QPT) [16]. As a result, a fidelity value of $F = 0.933$ was obtained. Briefly, this tomographic scheme consists of preparing $\sim d^2$ states that conform a basis of the space of lineal operators acting on $\mathcal{H}$. Each of these states, after being affected by the experimental implementation of the process $\mathcal{E}_t$, is reconstructed by means of quantum state tomography (QST) [42]. Finally, an appropriate system of linear equations is inverted to give the process matrix χ_{exp}.

In addition, we have analyzed how the quality in the reconstruction of the matrix χ affects the possibility of estimating a quantum state after the corresponding channel. To this purpose, we performed QST for a large number of pure states, ρ_{in}, randomly chosen on $\mathcal{H}$ and prepared by SLM_1, after being affected by the experimental implementation of the process $\mathcal{E}_t$. We compared each reconstructed state, ρ_{out}, with the predicted one by the action of the process $\mathcal{E}_{\text{exp}}$, previously obtained by means of the SEQPT method. As a figure of merit we used the fidelity between these two states, $F[\rho_{\text{out}}, \mathcal{E}_{\text{exp}}(\rho_{\text{in}})]$. In Fig. 5(a) we show the histogram of the fidelity for 250 of such

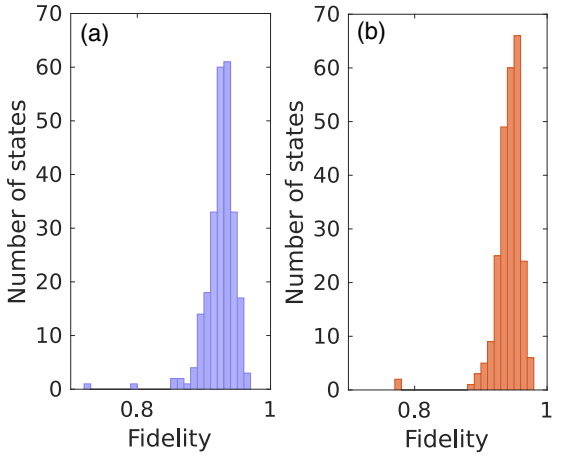

FIG. 5. Histogram of the state fidelity $F[\rho_{\text{out}}, \mathcal{E}_{\text{exp}}(\rho_{\text{in}})]$ between the density matrix ρ_{out}, obtained after performing QST of a given initial state ρ_{in} affected by the implemented process, and the expected density matrix $\mathcal{E}_{\text{exp}}(\rho_{\text{in}})$ corresponding to the same initial state under the action of the map $\mathcal{E}_{\text{exp}}$, obtained after performing QPT of the implemented process. Obtained fidelity in the case in which tensor product SEQPT (a) or standard QPT (b) was performed. For each histogram, 250 arbitrary states of dimension $d = 6$ were prepared and measured.

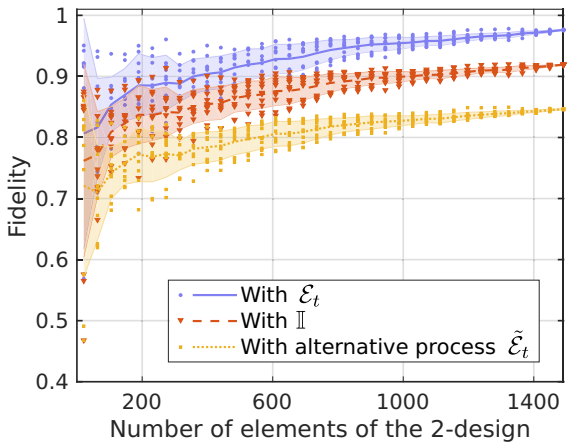

FIG. 6. Fidelity in the reconstruction of the implemented process for an increasing sampling on the elements of the tensor product of 2-design. The sampling is performed only to reconstruct the 21 nonzero elements characterizing the target process $\mathcal{E}_t$. The different markers represent the fidelity values between the reconstructed process and the different target processes $\mathcal{E}_{\text{target}}$. The mean value of the fidelity is indicated by a continuous line ($\mathcal{E}_{\text{target}} = \mathcal{E}_t$), a dashed line ($\mathcal{E}_{\text{target}} = \mathbb{I}$), or a dotted line ($\mathcal{E}_{\text{target}} = \tilde{\mathcal{E}}_t$). In each case, the shaded areas correspond to the standard deviation.

states. In Fig. 5(b) we present the analogous histogram for the case in which the process $\mathcal{E}_{\text{exp}}$ was reconstructed by means of the standard QPT method. The average state fidelity in the case of SEQPT is $\langle F_{\text{seqpt}} \rangle = 0.925$, with a standard deviation of $\sigma_F = 0.024$, while in the case of standard QPT we obtain $\langle F_{\text{sqpt}} \rangle = 0.942$ and a similar standard deviation σ_F. Although the mean values of the state fidelity are different between the two methods, they are within the estimated standard deviation.

The main aspect of the QPT method that we study here is that it is both *selective* and *efficient*. The selective property makes it ideally suited to reconstruct target processes with few nonzero matrix elements. The target process $\mathcal{E}_t$ that we have implemented has, in the selected basis, 21 nonzero elements over a total of 1296 elements of the matrix χ. The efficiency property allows us to estimate each element $\chi^{i_1 i_2}_{j_1 j_2}$ by averaging only on a subset of size $M \leqslant |X_\otimes|$. To test these properties experimentally we have randomly chosen different subsets of increasing size M, one for each nonzero coefficient $\chi^{i_1 i_2}_{j_1 j_2}$, from the same data set used in the reconstruction of the full matrix. Figure 6 shows the Choi-Jamiolkowski fidelity $F(\rho_{\text{theo}}, \rho_{\text{exp}})$ between the target process $\mathcal{E}_t$ and the reconstructed one, $\mathcal{E}_{\text{exp}}$, as a function of the total number of the sampled states, $21 \times M$. To analyze the effect of the sample, we reconstructed each of the nonzero coefficients $\chi^{i_1 i_2}_{j_1 j_2}$ from several random permutations of size M in the set $X_\otimes$, which has a total of 72 elements. Then, each point in the graphic illustrates one particular permutation. It is remarkable that less than 400 measurement settings were needed to reconstruct this processes with a fidelity above 0.9, from a total of $21 \times 72 = 1512$ measurement settings and a total of 2592 for a full tomography. We also show the fidelity with respect to two other target process: the identity process $\mathbb{I}$ (dashed line) and a process $\tilde{\mathcal{E}}_t$ (dotted line) close to $\mathcal{E}_t$, which has the same Kraus decomposition of Eq. (19), but corresponding to adding a constant phase shift, $\Delta\tilde{\varphi} = \Delta\varphi + 1$ rad. We can conclude that sampling only 10 elements in $X_\otimes$ per nonzero coefficient $\chi^{i_1 i_2}_{j_1 j_2}$ is enough to differentiate $\mathcal{E}_t$ from $\tilde{\mathcal{E}}_t$, while around 50 elements are needed to differentiate $\mathcal{E}_t$ from the identity process.

V. CONCLUSIONS

In this work, we have presented an experimental realization of the tensor product scheme for the SEQPT protocol. This generalizes the original SEQPT method, allowing one to efficiently and selectively characterize any quantum process in arbitrary dimension d. We successfully reconstructed a physical target process in dimension $d = 6$, which is the smallest dimension for which this SEQPT extension becomes relevant. We explicitly showed how to experimentally build each step of the algorithm and tested the method in a photonic platform, showing that it has a performance comparable to that of the established standard QPT for the same experimental conditions.

In addition, we verified that the reconstruction can be carried out selectively and efficiently. For that matter, we randomly sampled an increasing number of elements of the tensor product of 2-designs to obtain the nonzero elements of the target process matrix, which provided enough information to distinguish it from other processes. The resulting fidelity is above 0.9 by sampling only a small fraction of the total set of states.

ACKNOWLEDGMENTS

This work was supported by Universidad de Buenos Aires (UBACyT Grant No. 20020170100564BA). Q.P.S. was supported by a CONICET Fellowship.

[1] C. Outeiral, M. Strahm, J. Shi, G. M. Morris, S. C. Benjamin, and C. M. Deane, WIREs Comput. Mol. Sci. **11**, e1481 (2020).

[2] GoogleAIQuantum, Science **369**, 1084 (2020).

[3] S. K. Liao, W. Q. Cai, W. Y. Liu, L. Zhang, Y. Li, J. G. Ren, J. Yin, Q. Shen, Y. Cao, Z. P. Li, F. Z. Li, X. W. Chen, L. H. Sun, J. J. Jia, J. C. Wu, X. J. Jiang, J. F. Wang, Y. M. Huang, Q. Wang, Y. L. Zhou *et al.*, Nature (London) **549**, 43 (2017).

[4] N. Gisin and R. Thew, Nat. Photonics **1**, 165 (2007).

[5] D. Llewellyn, Y. Ding, I. I. Faruque, S. Paesani, D. Bacco, R. Santagati, Y.-J. Qian, Y. Li, Y.-F. Xiao, M. Huber, M. Malik, G. F. Sinclair, X. Zhou, K. Rottwitt, J. L. O'Brien, J. G. Rarity, Q. Gong, L. K. Oxenlowe, J. Wang, and M. G. Thompson, Nat. Phys. **16**, 148 (2020).

[6] M. Mohseni, A. T. Rezakhani, and D. A. Lidar, Phys. Rev. A **77**, 032322 (2008).

[7] A. G. Kofman and A. N. Korotkov, Phys. Rev. A **80**, 042103 (2009).

[8] S. J. Devitt, W. J. Munro, and K. Nemoto, Rep. Prog. Phys. **76**, 076001 (2013).

[9] J. B. Altepeter, D. Branning, E. Jeffrey, T. C. Wei, P. G. Kwiat, R. T. Thew, J. L. O'Brien, M. A. Nielsen, and A. G. White, Phys. Rev. Lett. **90**, 193601 (2003).

[10] Y. Kim, Y. S. Kim, S. Y. Lee, S. W. Han, S. Moon, Y. H. Kim, and Y. W. Cho, Nat. Commun. **9**, 192 (2018).

[11] Z. W. Wang, Y. S. Zhang, Y. F. Huang, X. F. Ren, and G. C. Guo, Phys. Rev. A **75**, 044304 (2007).

[12] R. C. Bialczak, M. Ansmann, M. Hofheinz, E. Lucero, M. Neeley, A. D. Oconnell, D. Sank, H. Wang, J. Wenner, M. Steffen, A. N. Cleland, and J. M. Martinis, Nat. Phys. **6**, 409 (2010).

[13] T. Yamamoto, M. Neeley, E. Lucero, R. C. Bialczak, J. Kelly, M. Lenander, M. Mariantoni, A. D. O'Connell, D. Sank, H. Wang, M. Weides, J. Wenner, Y. Yin, A. N. Cleland, and J. M. Martinis, Phys. Rev. B **82**, 184515 (2010).

[14] A. M. Childs, I. L. Chuang, and D. W. Leung, Phys. Rev. A **64**, 012314 (2001).

[15] M. Riebe, K. Kim, P. Schindler, T. Monz, P. O. Schmidt, T. K. Körber, W. Hänsel, H. Häffner, C. F. Roos, and R. Blatt, Phys. Rev. Lett. **97**, 220407 (2006).

[16] M. A. Nielsen and I. L. Chuang, *Quantum Computing and Quantum Information* (Cambridge University, Cambridge, England, 2000).

[17] A. Bendersky, F. Pastawski, and J. P. Paz, Phys. Rev. Lett. **100**, 190403 (2008).

[18] A. Bendersky, F. Pastawski, and J. P. Paz, Phys. Rev. A **80**, 032116 (2009).

[19] C. T. Schmiegelow, A. Bendersky, M. A. Larotonda, and J. P. Paz, Phys. Rev. Lett. **107**, 100502 (2011).

[20] A. Gaikwad, D. Rehal, A. Singh, Arvind, and K. Dorai, Phys. Rev. A **97**, 022311 (2018).

[21] W. K. Wootters and B. D. Fields, Ann. Phys. **191**, 363 (1989).

[22] I. D. Ivonovic, J. Phys. A: Math. Gen. **14**, 3241 (1981).

[23] T. Dur, B.-G. Englert, I. Bengtsson, and K. Życzkowski, Int. J. Quantum. Inf. **08**, 535 (2010).

[24] I. Perito, A. J. Roncaglia, and A. Bendersky, Phys. Rev. A **98**, 062303 (2018).

[25] G. Cañas, M. Arias, S. Etcheverry, E. S. Gómez, A. Cabello, G. B. Xavier, and G. Lima, Phys. Rev. Lett. **113**, 090404 (2014).

[26] S. Etcheverry, G. Cañas, E. S. Gómez, W. A. T. Nogueira, C. Saavedra, G. B. Xavier, and G. Lima, Sci. Rep. **3**, 2316 (2013).

[27] M. A. Solís-Prosser, M. F. Fernandes, O. Jiménez, A. Delgado, and L. Neves, Phys. Rev. Lett. **118**, 100501 (2017).

[28] D. Goyeneche, G. Cañas, S. Etcheverry, E. S. Gómez, G. B. Xavier, G. Lima, and A. Delgado, Phys. Rev. Lett. **115**, 090401 (2015).

[29] Q. P. Stefano, L. Rebón, S. Ledesma, and C. Iemmi, Opt. Lett. **44**, 2558 (2019).

[30] J. J. M. Varga, L. Rebón, Q. Pears Stefano, and C. Iemmi, Opt. Lett. **43**, 4398 (2018).

[31] A. Klappenecker and M. Rötteler, Proc. Int. Symp. Inf. Theory **2005**, 1740 (2005).

[32] L. Neves, G. Lima, J. G. Aguirre Gómez, C. H. Monken, C. Saavedra, and S. Pádua, Phys. Rev. Lett. **94**, 100501 (2005).

[33] G. Lima, A. Vargas, L. Neves, R. Guzmán, and C. Saavedra, Opt. Express **17**, 10688 (2009).

[34] M. A. Solís-Prosser, A. Arias, J. J. M. Varga, L. Rebón, S. Ledesma, C. Iemmi, and L. Neves, Opt. Lett. **38**, 4762 (2013).

[35] J. Leach, M. J. Padgett, S. M. Barnett, S. Franke-Arnold, and J. Courtial, Phys. Rev. Lett. **88**, 257901 (2002).

[36] G. Lima, L. Neves, R. Guzmán, E. S. Gómez, W. A. T. Nogueira, A. Delgado, A. Vargas, and C. Saavedra, Opt. Express **19**, 3542 (2011).

[37] M. Malik, M. Mirhosseini, M. P. J. Lavery, J. Leach, M. J. Padgett, and R. W. Boyd, Nat. Commun. **5**, 3115 (2014).

[38] A. Marquez, C. Iemmi, I. S. Moreno, J. A. Davis, J. Campos, and M. J. Yzuel, Opt. Eng. **40**, 2558 (2001).

[39] J. J. Sylvester, Johns Hopkins University Circulars I, pp. 241–242 (1982); *ibid.* II (1883), p. 46; *ibid.* III (1884), pp. 7–9. Summarized in *The Collected Mathematics Papers of James Joseph Sylvester* (Cambridge University, Cambridge, England, 1909), Vol. III.

[40] A. Singh and S. M. Carroll, arXiv:1806.10134v2.

[41] G. C. Knee, E. Bolduc, J. Leach, and E. M. Gauger, Phys. Rev. A **98**, 062336 (2018).

[42] R. T. Thew, K. Nemoto, A. G. White, and W. J. Munro, Phys. Rev. A **66**, 012303 (2002).